Band-gap control of graphenelike borocarbonitride *g*-BC_6N bilayers by electrical gating

A. Bafekry [1,*] and C. Stampfl [2,†]
[1]*Department of Physics, University of Guilan, 41335-1914 Rasht, Iran*
[2]*School of Physics, The University of Sydney, New South Wales 2006, Australia*

(Received 18 April 2020; accepted 19 October 2020; published 9 November 2020)

Motivated by the recent successful formation of boron and nitrogen-doped graphene, using density-functional-theory calculations, we investigate the atomic and electronic structure of bilayers of a graphene-like borocarbonitride (g-BC_6N@2L). Although pristine graphene is a semimetal, the single layer of g-BC_6N is a semiconductor with a direct band gap of 1.3 eV, as is the bilayer g-BC_6N@2L, which has a slightly smaller band gap of 1.2 eV. Systematic calculations for the bilayer structure, to investigate the effect of an electric field (E field), reveal that with increase of E-field, from 0.1 to 0.6 (V/Å), the band gap decreases linearly for both parallel and antiparallel E-field directions. For larger E fields (>0.6 V/Å), we find the formation of dual narrow band gaps of 50 meV (for parallel) and 0.4 eV (for antiparallel). The shape of energy bands is preserved and the value of band gaps are constant in both E-field directions. Our results indicate that monolayer and bilayer graphene-like borocarbonitride (g-BC_6N) is an interesting system which may find applications in future low-dissipation, high-speed nanoelectronic devices.

DOI: 10.1103/PhysRevB.102.195411

I. INTRODUCTION

The existence of high-mobility charge carriers in graphene has placed it at the forefront of recent intensive research efforts. In particular, research aimed to develop high-speed graphene-based electronic devices has been growing exponentially [1]. A field-effect transistor constructed using graphene (GFET) [2] is a promising candidate for applications in flexible electronic circuits [3]. However, the absence of a band gap in graphene limits the performance of GFETs in optoelectronic device applications. For the realization of a high on/off current ratio in FETs, it is essential that the ultrathin material used should possess a finite, suitable band gap. Recently, a number of approaches have been explored for introducing and controlling the band gap in graphene structures, in addition to searching for novel ultrathin semiconductors [4]. Approaches include the adsorption of molecules and atoms [5,6], dimensional reduction and structural engineering [7], and application of external effects such as a strong electric field [8]. Also, twisted graphene bilayers with intercalated alkali metals have been shown to afford the opening and engineering of a band gap [9]. Importantly, the method must provide sufficiently stable systems with a reproducible intrinsic band gap. A solution for such a problem, proposed theoretically, is sublattice asymmetry doping or unbalanced sublattice doping in the crystal structure. The important point is the introduction of impurities into one of the available sublattices of graphene [10,11], instead of both.

According to the proposed reports, when the impurities randomly substitute on the carbon sites in two sublattices, the resultant graphene-based structure is still gapless. In contrast, as the impurity atoms are randomly incorporated into single atomic sites in the graphene sublattice, a considerable band gap is opened in the doped structure [12], which indeed improves the transport properties of conventional GFETs [11]. Significant effort has been given to introducing a tunable band gap in graphene using various methods; these include chemisorption [13–17], substitutional doping with heteroatoms [18,19], applying electric fields [20,21] and growing graphene on substrates such as SiO_2 and SiC [22,23]. Interestingly, foreign atoms, in particular B and N, have been widely investigated in order to change its electronic properties [24–28]. B and N are neighboring elements of carbon in the periodic table and have similar mass and size to that of carbon. Incorporation of B or N has been shown to be an effective approach to open the band gap in the vicinity of the Dirac point, however, it may introduce the band gap above or below the Fermi level [25]. As compared to the N-N or B-B bond lengths, the N-B bond length is similar to the C-C bond length, which makes B-N a good choice to replace a C-C bond without causing significant distortions in the two-dimensional (2D) lattice. The introduction of N-B into graphene breaks the symmetry of the unit cell [29], and can result in the introduction of a band gap at the Fermi energy [30]. The effect of concentration has been investigated by Fan *et al.* [31] by varying the number of host atoms, and Manna and Pati [32] have shown that the patterning of h-BN and graphene sheets with insulating and/or semiconducting $B_xN_y(C_z)$ nanodomains of different sizes and geometrical shapes (h-BN sheet) can notably change the magnetic and electronic properties. Nitrogen and boron-doped single-layer graphene and bilayer graphene (BLG) have been experimentally synthesized by arc discharge using boron-packed graphite electrodes in the presence of ammonia [24]. Also,

*bafekry.asad@gmail.com
†catherine.stampfl@sydney.edu.au

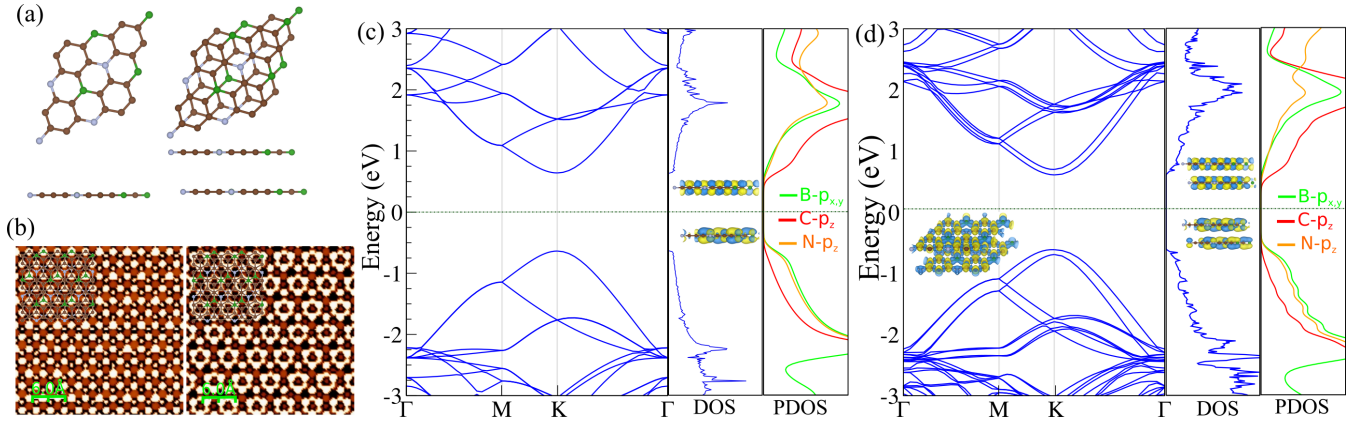

FIG. 1. (a) Optimized structures of g-BC_6N) (left) and the bilayer (right). Here green, gray, and brown circles represent boron, nitrogen, and carbon atoms, respectively. (b) *Ab initio* STM images of bilayer g-BC_6N for two bias voltages: +1 V (left), −1 V (right). Electronic band structure and corresponding density of states (DOS) and partial DOS (PDOS) of g-BC_6N for the (c) monolayer and (d) bilayer. The zero of energy is at the Fermi level. The electronic states of the valence band maximum (VBM) and conduction band minimum (CBM) orbitals are shown in the inset in the DOS.

in an earlier study, the synthesis of a layered borocarbonitride with stoichiometry BC_6N was reported [33], but the crystal structure has not been identified. More recently, BN-codoped nanographene has been synthesized via multiple borylation reactions of triarylamines representing a BCN system without inversion symmetry [34]. *Ab initio* calculations for the doped BLG systems consistently explained the p-and n-type behavior in graphene and the scanning tunneling microscopy (STM) images were successfully supported [35,36]. A tight-binding approach has also been employed to study doped BLG systems [37,38]. In the absence of an electric field, it was shown that the band gap of BLG can be chemically tuned by doping [18,38,39] and functionalization [40,41]. Another approach by which the band gap can be tuned is by applying strain to the doped BLG [42]. Although two-dimensional materials hold significant potential for many applications, it will be necessary to tune their intrinsic properties. Several approaches have been considered to change the electronic structure of two-dimensional materials such as substitutional doping, defect engineering, application of an electric field or strain or surface functionalization by adatoms, e.g., Refs. [43–46].

The physical properties of various B/N-doped graphene structures has been reported recently on the basis of *ab initio* calculations in Refs. [47,48] where a range of concentrations (4–24%) and geometries was considered. An opening of the band gap was found, with varying values depending on the doping site and concentration. Also, recent first-principles calculations have been reported for the electronic properties of monolayer g-BC_6N, in which the B and N atoms occupy opposite vertices of the graphene hexagon [cf. Fig. 1(a)] [49–53], where the former reported a band gap of 1.273 eV, and the latter of 1.276 eV, and 1.833 eV when using the HSE06 hybrid functional. To date, however, the effect of an electric field on the band gap has not been investigated.

In this work, we investigate the electronic properties of monolayer g-BC_6N and bilayer g-BC_6N@2L by *ab initio* calculations and in particular consider the effect of application of an electric field oriented perpendicular to the plane of the surface for both the parallel and antiparallel directions. We show that the band gap of g-BC_6N@2L can be strongly modified by applying an electric field and there is a difference between the orientations of the field.

II. METHOD

We use density functional theory (DFT) with the generalized gradient approximation for the exchange-correlation functional as proposed by Perdew-Burke-Ernzerhof (GGA-PBE) [54], together with norm-conserving pseudopotentials [55] as implemented in OpenMX package. The eigenfunctions and eigenvalues of the Kohn-Sham equations are obtained self-consistently using norm-conserving pseudopotentials, and pseudoatomic orbitals (PAOs) [56,57]. The wave functions are expanded as a linear combination of multiple pseudoatomic orbitals (LCPAOs). The integration over the Brillouin zone is performed using a **k**-point mesh of $12 \times 12 \times 1$ in the Monkhorst-Pack scheme for the (4×4) unit cell used in the present work [58]. The monolayer and bilayer structures are modelled as a periodic slab with a vacuum layer of 20 and 25 Å, respectively, between them in order to avoid interactions between repeating layers. A quasi-Newton algorithm is used to determine the ground state structure which was relaxed until the residual forces on the atoms were smaller than 1 meV/Å. In order to describe the van der Waals (vdW) interaction, we adopted the method of Grimme (DFT-D3) [59], which has been shown to be reliable for describing the long-range vdW interactions.

III. MONOLAYER g-BC_6N

Here we study the electronic structure of g-BC_6N and g-BC_6N@2L. The optimized structures are shown in the left and right of Fig. 1(a), respectively. In Refs. [49,50] dispersion calculations showed no imaginary frequencies for the monolayer system, indicating the structure is dynamically stable.

Calculated STM images of g-BC_6N@2L for two bias voltages +1 V, −1 V are shown in the left and right of Fig. 1(b), respectively. The lattice parameter of the optimized

(4×4) supercell used for the calculations of g-BC_6N and g-BC_6N@2L is determined to be 10.024 Å, while the C-C, C-B, and C-N bond lengths are 1.42, 1.48, and 1.46 Å, respectively. The bond angle between atoms is ∼120°, displaying the characteristics of sp^2 hybridization. Our results show that the introduction of B/N into graphene, causes only a weak structural distortion. The density of states (DOS), projected density of states (PDOS) and electronic band structure of g-BC_6N is shown in Fig. 1(c). It can be seen that the introduction of B and N into the graphene lattice transforms thet semimetallic character of pristine graphene into a semiconductor. The Dirac-point disappears completely and opens a direct band gap of 1.3 eV at the K point. Furthermore, from the PDOS in Fig. 1(c), we can see that the VBM originates from B-$p_{x,y}$ and N-p_z orbitals, while the CBM originates from the C-p_z orbitals. Insets in Figs. 1(c) and 1(d) show the electronic states at the VBM and CBM orbitals.

By stacking two g-BC_6N layers vertically, we form a g-BC_6N@2L heterobilayer. Before studying the electronic properties, we consider the most stable geometry. This is obtained by placing different stacking (AA and AB) of the layers on the each other [see Figs. S1(a) and S1(b) in the Supplemental Material [60]. With full structural optimization, we find the most stable stacking arrangement (as the minimum energy configuration among the different geometries considered) is the AB-stacking arrangement (Fig. S1(b) [60]) where a B atom from the upper layer is vertically above a C atom in the lower layer. We calculate the binding energy as a function of interlayer distances and find that the equilibrium distance occurs at 3.44 Å (see Fig. S1(c) [60]). We investigate the thermal stability of g-BC_6N@2L by performing *ab-inito* molecular dynamic (AIMD) simulations (see Fig. S2 [60]). We start with the optimized structure at 0 K, and the temperature is increased to 300 K for a 2 ps total simulation time. As can be noticed from the snapshots, apart from minor distortions, the crystal structure is preserved, predicting thermal stability at 300 K. The electronic band structure, DOS and PDOS of g-BC_6N@2L is shown in Fig. 1(d). It can be seen that the system is a direct semiconductor with a band gap of 1.2 eV. The VBM mainly is largely composed of B-$p_{x,y}$ and N-p_z orbitals, while the CBM originates from the C-p_z orbital, similar to monolayer g-BC_6N.

IV. EFFECT OF AN ELECTRIC FIELD ON THE ELECTRONIC PROPERTIES OF g-BC_6N@2L

With regard to potential device applications, the ability to tune the electronic structure by, e.g., controlling the Fermi level via electric field (E field) is highly desirable. The presence of the interlayer distance in g-BC_6N@2L leads to a potential difference between the two atomic layers, which is intrinsically useful in tuning the electronic properties. In the following, the effect of an E field on the electronic properties is investigated. The band structure of g-BC_6N@2L in the presence of a perpendicular E field is shown in Fig. 2. The strength of the E field >0 (<0) denotes parallel (antiparallel) to the z axis. Notice that the electronic structure is strongly modified by application of an E field. When applying a parallel E field its direct band gap decreases from 1.2 eV (0 V/Å) to 0.1 eV (0.5 V/Å). Surprisingly, for increase of the electric field to

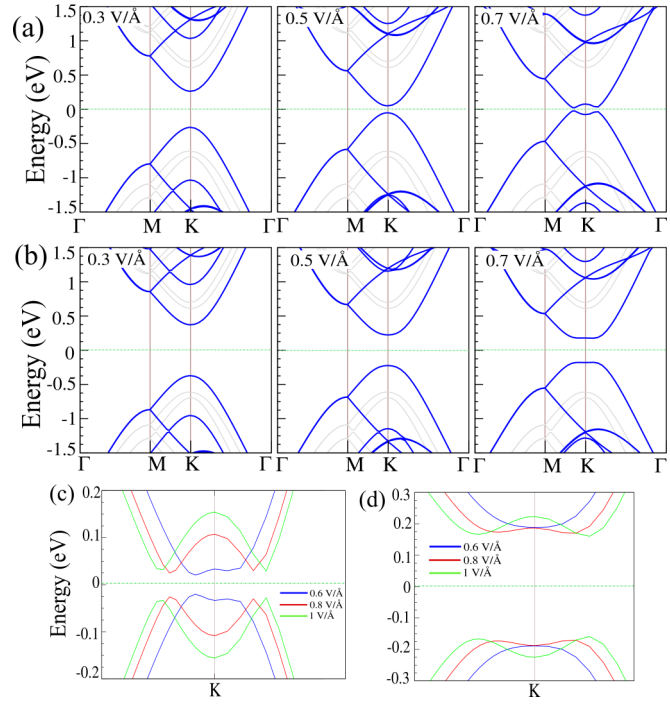

FIG. 2. Electronic band structure of g-BC_6N@2L for various values of an applied electric field in the parallel [(a) and (c)] and antiparallel [(b) and (d)] directions. The positive (negative) electric field denotes parallel (antiparallel) to the z axis in the normal direction, where the strength varies from 0 to 1 V/Å. The zero of energy is set at the Fermi level.

0.6 V/Å, we see a dual narrow band gap of ∼50 meV [see Fig. 2(c)]. With further increase of E field from 0.6 to 1 V/Å, the VBM and CBM at the K point do not vary significantly so the dual band gap is maintained at about 50 meV.

The electronic response of g-BC_6N@2L in the antiparallel direction is similar to that in the parallel direction, except that the band gap is not so significantly reduced. Specifically, the negative E field is able to decrease the band gap to 0.95 eV (at 0.2 V/Å), 0.6 eV (at 0.4 V/Å), 0.45 eV (at 0.5 V/Å). Interestingly, the band gap reaches 0.4 eV at 0.6 V/Å and for further increase of the E field to 1 V/Å, the shape of the dual narrow band gap is preserved and from 0.6 to 1 V/Å, the band gap stays constant at ∼0.4 eV. The intensity map of the band structure in the absence (left) as well as in the presence of a parallel (middle) and antiparallel (right) field with a strength of 0.6 V/Å is shown in Fig. 3(a). The band gap plotted as a function of the E field is shown in Fig. 3(b). This behavior can be understood in terms of the charge transfer taking place between the dopant atoms and the C atoms of the host. Examining the charge transfer reveals that the B atoms receive electron density, while C atoms donate it. Therefore, the negatively charged B atoms reside on top of positively charged C atoms, generating a small built-in electric field. When the direction of the electric field is changed (parallel to antiparallel), the internal (built-in) electric field strengthens or weakens. The electronic band gap is therefore, affected differently for the two E field orientations. In Fig. S3 [60], the total charge transfer between the layers (per unit cell) is plotted as a function of the electric field. For zero field, there

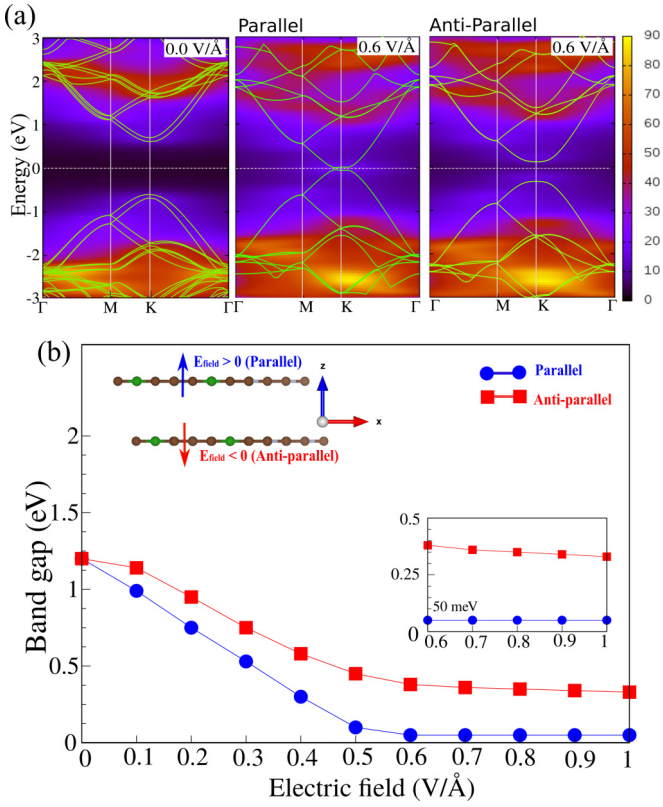

FIG. 3. (a) Intensity map of the band structure of g-BC_6N@2L in the absence (left) as well as in the presence of a parallel (middle) and antiparallel (right) electric field with strength of 0.6 V/Å. (b) Band gap of g-BC_6N@2L as a function of E field. The atomic structure and E field are shown in the inset.

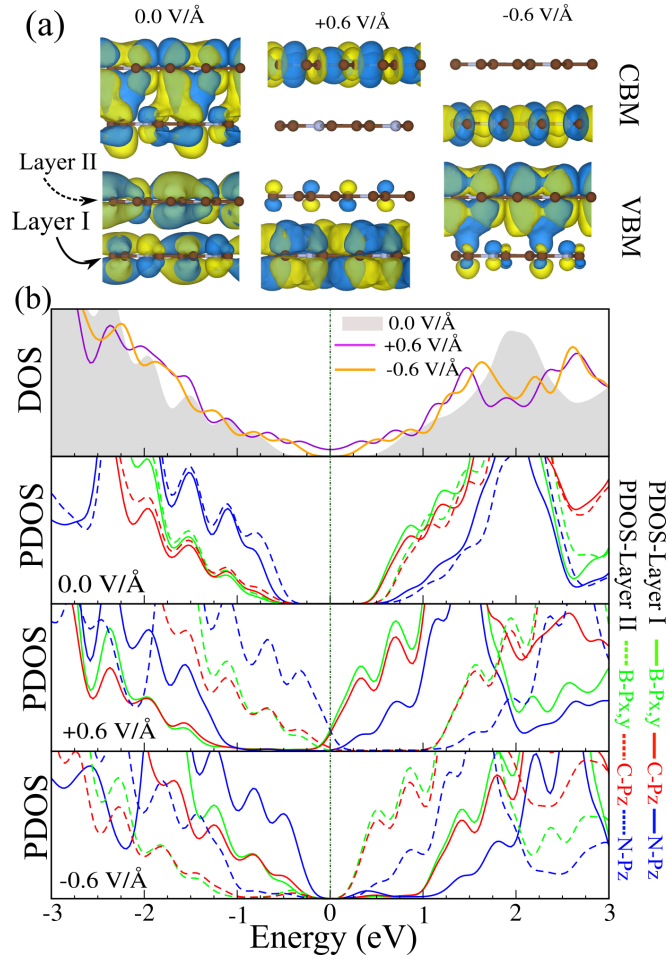

FIG. 4. (a) Electronic states at the VBM and CBM orbitals and (b) DOS and PDOS of g-BC_6N@2L for parallel and antiparallel E fields with a strength of 0.6 V/Å. The zero of energy is at Fermi level.

is a net charge transfer of 0.02e. Analogous calculations for monolayer g-BC_6N shows insignificant variation of the band gap with applied electric field.

The electronic states at the VBM and CBM, and DOS and PDOS of g-BC_6N@2L for parallel and antiparallel E fields with a strength of 0.6 V/Å are shown in Figs. 4(a) and 4(b). This electronic phase modification is due to the Stark effect, as a consequence of the energy shift caused by the difference in electrostatic potential between the two layers that are separated by a distance of 3.44 Å. The response of the electronic band structure of a material to an E field is mostly determined by the atomic orbital contributions to the band edges of the material. From the DOS and PDOS of g-BC_6N@2L in Fig. 4(b), we can see that the VBM and CBM originate from B/N and C atomic orbitals, respectively. Notice that the VBM is dominated by in-plane B-$p_{x,y}$ orbitals and out-of-plane of N-p_z orbitals, while the C-p_z orbital does not have any contribution. In contrast, the CBM is dominated by the out-of-plane of C-p_z orbitals. Apparently, an applied out-of-plane E field on the g-BC_6N@2L both the VBM and CBM are affected by the applied field due to out-of-plane (p_z) orbitals contributing to both band edges. Overall, depending on the atomic orbital characters of the band edges, the material responds differently to the external effects.

We also consider other doping patterns of the bilayer system including the N atom in the upper layer on top of a C atom in the lower layer and a C atom in the upper layer on top of a C atom in the lower layer. The corresponding electronic band structures for various values of applied an electric field in the parallel and antiparallel directions are shown in Figs. S4(a) and S4(b), S4(c) and S4(d), and Figs. S5(a) and S5(b), respectively [60]. Top and side views of the optimized structures are shown in the insets. We can see that the response of the band gap to the applied E field is the same for both parallel and antiparallel fields in accordance with the stacking symmetry.

V. CONCLUSION

In conclusion, we investigated the electronic and atomic properties of a graphene-like borocarbonitride, g-BC_6N and its bilayer, including the effect of an applied electric field using first-principle calculations. Monolayer, g-BC_6N has been reported previously to be dynamically stable through calculation of the phonon dispersion curves. This, together with the present *ab initio* molecular dynamics simulations at 300 K, which find the g-BC_6N and g-BC_6N@2L structures are maintained, suggests it may be possible to synthesize such structures experimentally. The single-layer g-BC_6N structure

has a direct band gap of 1.3 eV while that of the bi-layer system has a band gap of 1.2 eV. Additionally, the electronic properties of g-BC_6N@2L under application of a parallel (positive) and antiparallel (negative) E field is also studied. We find that the electronic properties can be strongly modified: On increasing the E field from 0.1 to 0.6 V/Å, the band gap decreases practically linearly. Interestingly, for the E field larger >0.6 V/Å, a dual narrow band gap develops with values of 50 meV (for parallel) and 0.4 eV (for antiparallel). Thus, depending on the direction of the applied E field, the band gap is modified to a slightly different degree. We expect that our theoretical study will stimulate further experimental research on this material in the future. Moreover, g-BC_6N@2L might be a candidate material for the realization of new graphene-based structures that have electrically tunable band gaps. This phenomena is of great interest for basic physics and is also a highly desirable characteristic for use in nanoscale device applications.

ACKNOWLEDGMENTS

This work was supported by the National Research Foundation of Korea grant funded by the Korea government (Grant No. NRF-2017R1A2B2011989).

[1] L. Banszerus, M. Schmitz, S. Engels, J. Dauber, M. Oellers, F. Haupt, K. Watanabe, T. Taniguchi, B. Beschoten, and C. Stampfer, Sci. Adv. **1**, e1500222 (2015).
[2] K. S. Novoselov, A. K. Geim, S. V. Morozov, D. Jiang, Y. Zhang, S. V. Dubonos, I. V. Grigorieva, and A. A. Firsov, Science **306**, 666 (2004).
[3] P. Nicholas, M. Inanc, H. James, and K. L. Shepard, Nano Lett. **13**, 121 (2013).
[4] B. Radisavljevic, A. Radenovic, J. Brivio, V. Giacometti, and A. Kis, Nat. Nanotechnol. **6**, 147 (2011).
[5] D. Haberer, L. Petaccia, Y. Wang, H. Quian, M. Farjam, S. A. Jafari, H. Sachdev, A. V. Federov, D. Usachov, D. V. Vyalikh, X. Liu, O. Vilkov, V. K. Adamchuk, S. Irle, M. Knupfer, B. Büchner, and A. Grüneis, Phys. Status Solidi B **248**, 2639 (2011).
[6] H. Y. Mao, Y. H. Lu, J. D. Lin, S. Zhong, A. T. S. Wee, and W. Chen, Prog. Surf. Sci. **88**, 132 (2013).
[7] H. Shen, Y. Shi, and X. Wang, Synth. Met. **210**, 109 (2015).
[8] X. Fengnian, D. B. Farmer, Yu-ming Lin, and P. Avouris, Nano Lett. **10**, 715 (2010).
[9] F. Symalla, S. Shallcross, I. Beljakov, K. Fink, W. Wenzel, and V. Meded, Phys. Rev. B **91**, 205412 (2015).
[10] J. A. Lawlor and M. S. Ferreira, Beilstein J. Nanotechnol. **5**, 1210 (2014).
[11] A. Lherbier, A. R. Botello-Méndez, and J.-C. Charlier, Nano Lett. **13**, 1446 (2013).
[12] V. M. Pereira, J. M. B. Lopes dos Santos, and A. H. Castro Neto, Phys. Rev. B **77**, 115109 (2008).
[13] X. Wang, X. Li, L. Zhang, Y. Yoon, P. K. Weber, H. Wang, J. Guo, and H. Dai, Science **324**, 768 (2009).
[14] E. Bekyarova, M. E. Itkis, P. Ramesh, C. Berger, M. Sprinkle, A. de Heer Walt, and R. C. Haddon, J. Am. Chem. Soc. **131**, 1336 (2009).
[15] J. O. Sofo, A. S. Chaudhari, and G. D. Barber, Phys. Rev. B **75**, 153401 (2007).
[16] I. Zanella, S. Guerini, S. B. Fagan, J. Mendes Filho, and A. G. Souza Filho, Phys. Rev. B **77**, 073404 (2008).
[17] J. Choi, Ki-jeong Kim, B. Kim, H. Lee, and S. Kim, J. Phys. Chem. C **113**, 9433 (2009).
[18] P. A. Denis, Chem. Phys. Lett. **492**, 251 (2010).
[19] J. Dai, J. Yuan, and P. Giannozzi, Appl. Phys. Lett. **95**, 232105 (2009).
[20] A. A. Avetisyan, B. Partoens, and F. M. Peeters, Phys. Rev. B **79**, 035421 (2009).
[21] K. F. Mak, C. H. Lui, J. Shan, and T. F. Heinz, Phys. Rev. Lett. **102**, 256405 (2009).
[22] P. Shemella and S. K. Nayak, Appl. Phys. Lett. **94**, 032101 (2009).
[23] P. Xiangyang and A. Rajeev, Nano Lett. **8**, 4464 (2008).
[24] L. S. Panchakarla, K. S. Subrahmanyam, S. K. Saha, A. Govindaraj, H. R. Krishnamurthy, U. V. Waghmare, and C. N. R. Rao, Adv. Mater. **21**, 4726 (2009).
[25] M. Wu, C. Cao, and J. Z. Jiang, Nanotechnology **21**, 505202 (2010).
[26] R. Faccio, L. Fernández-Werner, H. Pardo, C. Goyenola, O. N. Ventura, and Á. W. Mombrú, J. Phys. Chem. C **114**, 18961 (2010).
[27] Y.-B. Tang, L.-C. Yin, Y. Yang, X.-H. Bo, Y.-L. Cao, H.-E. Wang, W.-J. Zhang, I. Bello, S.-T. Lee, H.-M. Cheng, and C.-S. Lee, ACS Nano **6**, 1970 (2012).
[28] J. Gebhardt, R. J. Koch, W. Zhao, O. Höfert, K. Gotterbarm, S. Mammadov, C. Papp, A. Görling, H.-P. Steinrück, and T. Seyller, Phys. Rev. B **87**, 155437 (2013).
[29] P. Rani and V. K. Jindal, RSC Adv. **3**, 802 (2013).
[30] X. Deng, Y. Wu, J. Dai, D. Kang, and D. Zhang, Phys. Lett. A **375**, 3890 (2011).
[31] X. Fan, Z. Shen, A. Q. Liu, and J.-L. Kuo, Nanoscale **4**, 2157 (2012).
[32] A. K. Manna and S. K. Pati J. Phys. Chem. C **115**, 10842 (2011).
[33] M. Kawaguchi, Y. Wakukawa, and T. Kawano, Synth. Met. **125**, 259 (2002).
[34] K. Matsui, O. Susumu, K. Yoshiura, K. Nakajima, N. Yasuda, and T. Hatakeyama, J. Am. Chem. Soc. **140**, 1195 (2018).
[35] S.-O. Guillaume, B. Zheng, J.-C. Charlier, and L. Henrard, Phys. Rev. B **85**, 035444 (2012).
[36] Y. Fujimoto and S. Saito, Surf. Sci. **634**, 57 (2015).
[37] A. B. Kuzmenko, I. Crassee, D. van der Marel, P. Blake, and K. S. Novoselov, Phys. Rev. B **80**, 165406 (2009).
[38] H. Mousavi, J. Khodadadi, and M. Grabowski, Phys. B: Condens. Matter **530**, 90 (2018).
[39] M. G. Menezes, R. B. Capaz, and J. L. B. Faria, Phys. Rev. B **82**, 245414 (2010).
[40] D. W. Boukhvalov and M. I. Katsnelson, Phys. Rev. B **78**, 085413 (2008).
[41] T. Hu and I. C. Gerber, Chem. Phys. Lett. **616-617**, 75 (2014).
[42] Choi Seon-Myeong, Jhi Seung-Hoon, and Son Young-Woo, Nano Lett. **10**, 3486 (2010).

[43] A. Bafekry, M. Neek-Amal, and F. M. Peeters, Phys. Rev. B **101**, 165407 (2020).
[44] A. Bafekry and M. Neek-Amal, Phys. Rev. B **101**, 085417 (2020).
[45] A. Bafekry, C. Stampfl, and M. Ghergherehchi, Nanotechnology **31**, 295202 (2020).
[46] A. Bafekry, B. Akgenc, M. Ghergherehchi, and F. M. Peeters, J. Phys.: Condens. Matter **32**, 355504 (2020).
[47] P. Rani and V. K. Jindal, Appl. Nanosci. **4**, 989 (2014).
[48] M. Alattas and U. Schwingenschlogl, Sci. Rep. **8**, 17689 (2018).
[49] N. Abdullah, H. Rashid, C. Tang, A. Manolescu, and V. Gudmundsson, Phys. Lett. A **384**, 126807 (2020).
[50] X. Liu, X. Ma, H. Gao, X. Zhang, H. Ai, W. Li, and M. Zhao, Nanoscale **10**, 13179 (2018).
[51] B. Mortazavi, M. Shahrokhi, M. Raeisi, X. Zhuang, L. F. C. Pereira, and T. Rabczuk, Carbon **149**, 733 (2019).
[52] B. Mortazavi, M. Makaremi, M. Shahrokhi, Z. Fan, and T. Rabczuk, Carbon **137**, 57 (2018).
[53] B. Mortazavi, M. Shahrokhi, M. E. Madjet, M. Makaremi, S. Ahzi, and T. Rabczuk, Carbon **141**, 291 (2019).
[54] J. P. Perdew, K. Burke, and M. Ernzerhof, Phys. Rev. Lett. **77**, 3865 (1996).
[55] N. Troullier and J. L. Martins, Phys. Rev. B **43**, 1993 (1991).
[56] T. Ozaki, Phys. Rev. B **67**, 155108 (2003).
[57] T. Ozaki and H. Kino, Phys. Rev. B **69**, 195113 (2004).
[58] H. J. Monkhorst and J. D. Pack, Phys. Rev. B **13**, 5188 (1976).
[59] S. Grimme, J. Comput. Chem. **27**, 1787 (2006).
[60] See Supplemental Material at http://link.aps.org/supplemental/10.1103/PhysRevB.102.195411 includes of atomic structure, thermal stability, the total electron charge transfer, and band structure for various values of E field of g-BC_6N structure.